INTERNATIONAL JOURNAL FOR NUMERICAL AND ANALYTICAL METHODS IN GEOMECHANICS
Int. J. Numer. Anal. Meth. Geomech., **23**, 1309–1318 (1999)

SHORT COMMUNICATIONS

NUMERICAL INTEGRATION DURING FOURIER INTEGRAL ANALYSIS

R. W. I. BRACHMAN AND I. D. MOORE*

Geotechnical Research Centre, The University of Western Ontario, London, Ontario, N6A 5B9 Canada

SUMMARY

Numerical integration required during Fourier integral analysis is discussed. For the case of a long and prismatic elastic medium subject to three-dimensional loads applied at the surface (e.g. live load response of buried structures), the complexity of inverse integrals depends on the relative magnitude of the load width and the distance from the load in the longitudinal direction, as well as the longitudinal spacing of the loads. The inverse integrand of the applied surface loading is more difficult to evaluate compared to those for stresses and displacements. Selection of integration schemes based on successful inversion of the applied load provides accurate solutions of stress and displacement throughout the elastic body. The use of superposition when considering complex loading cases is beneficial. Copyright © 1999 John Wiley & Sons, Ltd.

KEY WORDS: Fourier integrals; numerical integration; three-dimensional analysis

1. INTRODUCTION

Various researchers are employing Fourier integral methods in the analysis of the three-dimensional elastic response of long prismatic soil structures (e.g. References 1–4). These procedures use Fourier integrals to transform the response in the longitudinal direction of the prismatic structure into harmonic form. Solutions are then assembled from harmonics through evaluation of the inverse integrals. This note describes the nature of these integrals and how Gaussian integration can be used in their calculation. Specific examples feature rectangular pressure distributions in the longitudinal direction.

2. FOURIER INTEGRALS

The description, theory and implementation of the three-dimensional semi-analytic finite element technique is as discussed by Moore and Brachman.[2] The Fourier integral approach removes the dependence upon the longitudinal spatial co-ordinate (i.e. z) in lieu of a transform variable, α. The

*Correspondence to: I.D. Moore, Geotechnical Research Centre, Department of Civil and Environmental Engineering, The University of Western Ontario, London, Ontario N6A 5B9, Canada

CCC 0363–9061/99/121309–10$17.50

Received 10 December 1997
Revised 16 April 1998

Fourier cosine integral of any function $f(\xi)$ is defined as

$$F_c(\alpha) = \int_0^\infty f(\xi)\cos(\alpha\xi)\,\mathrm{d}\xi \tag{1}$$

where $F_c(\alpha)$ is the Fourier cosine integral of $f(\xi)$, α the transform variable, and ξ the variable being transformed.

For example, vertical applied loads $f_y(z)$, displacements $u_y(z)$ and stresses $s_y(z)$ can be transformed by

$$F_{yc}(\alpha) = \int_0^\infty f_y(z)\cos(\alpha z)\,\mathrm{d}z \tag{2}$$

$$U_{yc}(\alpha) = \int_0^\infty u_y(z)\cos(\alpha z)\,\mathrm{d}z \tag{3}$$

$$S_{yc}(\alpha) = \int_0^\infty s_y(z)\cos(\alpha z)\,\mathrm{d}z \tag{4}$$

Harmonic finite element analysis can then be performed with a two-dimensional mesh (descretized in the x–y plane) to solve for the transformed displacements $U(\alpha)$ and stresses $S(\alpha)$ for specific values of α. Inverse integrals convert the harmonic response back to the Cartesian coordinate system. Inversions of the Fourier integrals to obtain the vertical applied load, displacement and stress quantities as a function of z are given by

$$f_y(z) = \frac{2}{\pi}\int_0^\infty F_{yc}(\alpha)\cos(\alpha z)\,\mathrm{d}\alpha \tag{5}$$

$$u_y(z) = \frac{2}{\pi}\int_0^\infty U_{yc}(\alpha)\cos(\alpha z)\,\mathrm{d}\alpha \tag{6}$$

$$s_y(z) = \frac{2}{\pi}\int_0^\infty S_{yc}(\alpha)\cos(\alpha z)\,\mathrm{d}\alpha \tag{7}$$

The integrands of equations (5)–(7) are functions of the transform variable α which can be evaluated for any particular z value of interest.

Elastic solutions for three-dimensional problems with long prismatic geometry can therefore be obtained using a two-dimensional finite element mesh and Fourier integrals. The successful application of the Fourier integral approach is contingent on the evaluation of these inverse Fourier integrals.

3. VARIATION OF APPLIED LOADING

Figure 1(a) illustrates the longitudinal variation of applied loading considered by Moore and Brachman.[2] It consists of two uniform patches of pressure of width w separated by a distance $2z_s$ acting on the ground surface. Vehicle loading of buried structures was simulated with w equal to the tire width and $2z_s$ as the axel length. Similar surface pressure distributions were considered by Fernando *et al.*[4] in their solution of a similar problem. A single patch of pressure of width $2w$ centred at $z = 0$ is modelled when z_s equals zero.

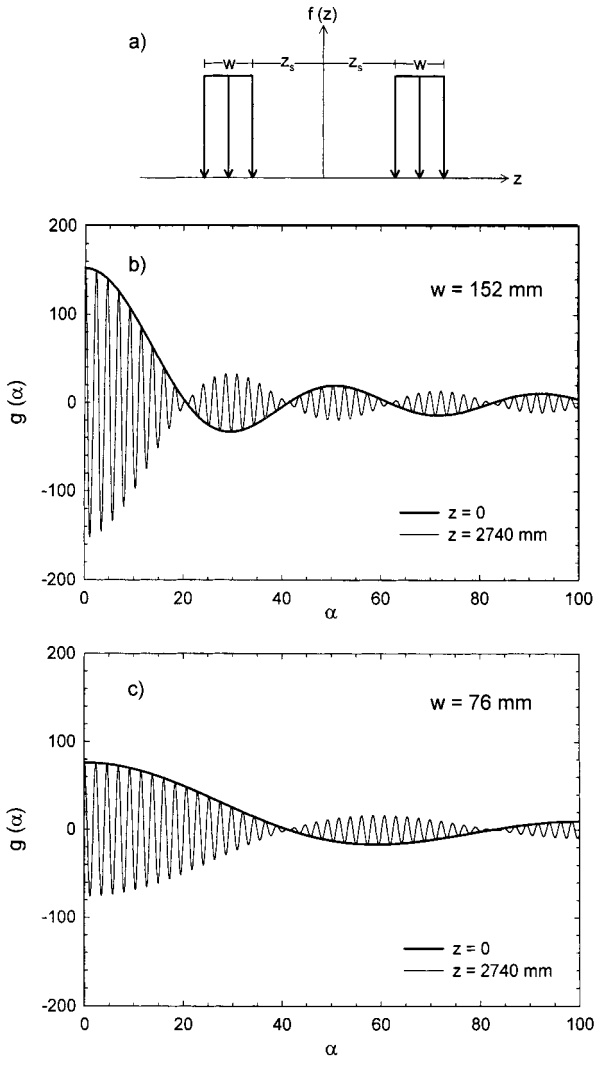

Figure 1. Inverse Fourier integrals for vertical applied loads. Generalized load function (a). Inverse integral for $z_s = 0$ with: $w = 152$ mm (b) and $w = 76$ mm (c)

More complex loading functions can also arise. Brachman *et al.*[5] have described how the Fourier integral technique can be used to assess the elastic ground response to load from a rigid rectangular footing. Here, the contact pressure under the footing was sub-divided into a series of uniformly loaded patches. Fourier integral analysis was used to assemble a flexibility relationship between patch pressures and displacements that was used to solve for the contact pressure. This analysis featured narrow patches of pressure characterized by the load variation of Figure 1(a), with z_s equal to zero and for several patch half-widths (i.e., w). The following sections are based on the solution requirements of Brachman *et al.*,[5] but are largely generic so that similar principles apply to most such Fourier integral applications.

4. TRANSFORMED LOADING FUNCTION

Of the transformed quantities, only the load variation in the longitudinal direction $f_y(z)$ is known at the outset of the analysis. The Fourier cosine integral of the general load function $f_y(z)$ depicted in Figure 1(a) is given by

$$F_{yc}(\alpha) = \frac{1}{\alpha}\left[\sin(z_s\alpha + w\alpha) - \sin(z_s\alpha)\right] \tag{8}$$

The inversion of the Fourier integral to obtain the original load function would involve performing the integral of equation (5). For a single patch of pressure (i.e. $z_s = 0$) this integral is equal to

$$f_y(z) = \frac{2}{\pi}\int_0^\infty \frac{\sin(w\alpha)\cos(z\alpha)}{\alpha}\,\mathrm{d}\alpha = \frac{2}{\pi}\int_0^\infty g(\alpha)\,\mathrm{d}\alpha \tag{9}$$

Figure 1 presents plots of the inverse integrand $g(\alpha)$ of equation (9) for two cases with load half-widths (w) equal to 152 and 76 mm (Figs. 1(b) and 1(c), respectively). In the limit, as α approaches zero, the integrand $g(\alpha)$ equals w; as α becomes very large (i.e. $\to \infty$), $g(\alpha)$ approaches zero. Between these limits, the amplitude of $g(\alpha)$ is inversely proportional to α. The latter two points are advantageous as the integral in equation (9) can be truncated at some sufficiently large value to facilitate numerical integration.

The zeros of the inverse integrand of equation (9) are functions of both w and z, and are controlled by the $\sin(w\alpha)$ and $\cos(z\alpha)$ components. Zeros are located at $\alpha = p\pi/w$ ($p = 1, 2, 3, \ldots$) for $z = 0$. Decreasing w results in an increase in the period of $g(\alpha)$. For non-zero z, additional roots arise from the $\cos(z\alpha)$ component and are located $\alpha = (2p-1)\pi/2z$ ($p = 1, 2, 3, \ldots$), as shown by the $z = 2740$ mm curves. The additional complexity of the integrand for larger z values is significant as greater numerical effort is required to invert the transform.

5. TRANSFORMED DISPLACEMENTS AND STRESSES

Transformed displacements $U(\alpha)$ and stresses $S(\alpha)$ are initially unknown and thus prohibit a direct examination of the inverse integrands as previously performed for the applied load. A simple test case involving a uniformly loaded patch was therefore analyzed to calculate the transformed displacements and stressed for various harmonic values. Results are shown for the case of a square patch of pressure ($z_s = 0$) of dimensions $2w \times 2w$ ($w = 152$ mm) acting on an elastic surface ($E = 50$ MPa, $v = 0{\cdot}3$). The two-dimensional (x–y) finite element mesh used for the analysis consisted of 52 six-noded triangles (Figure 2).

5.1. Transformed stresses

Figure 3(a) shown the stress integrand $S_{yc}(\alpha)\cos(\alpha z)$ for the vertical stress s_y, at point A near the surface. This plot is very similar to the integrand $g(\alpha)$ of the applied load previously shown in Figure 1(b). As expected the vertical stress near the surface is close to the applied surface traction. There is a 30 per cent decrease in amplitude of the function in Figure 3(a) relative to that in Figure 1(b) resulting from slight attenuation with depth. As previously, noted, the integrand becomes more complex for larger values of z, indicated by the $z = 2740$ mm curve in Figure 3(a).

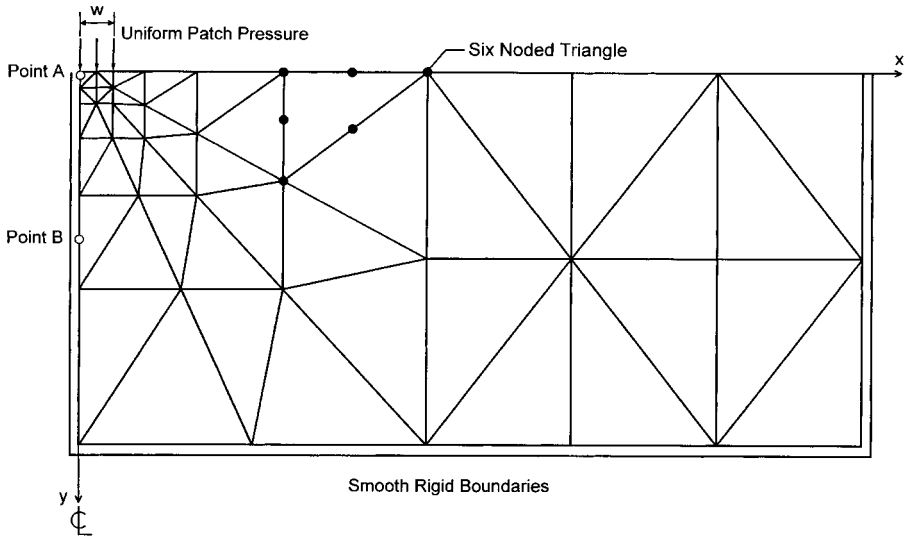

Figure 2. Two-dimensional finite element mesh used for test case

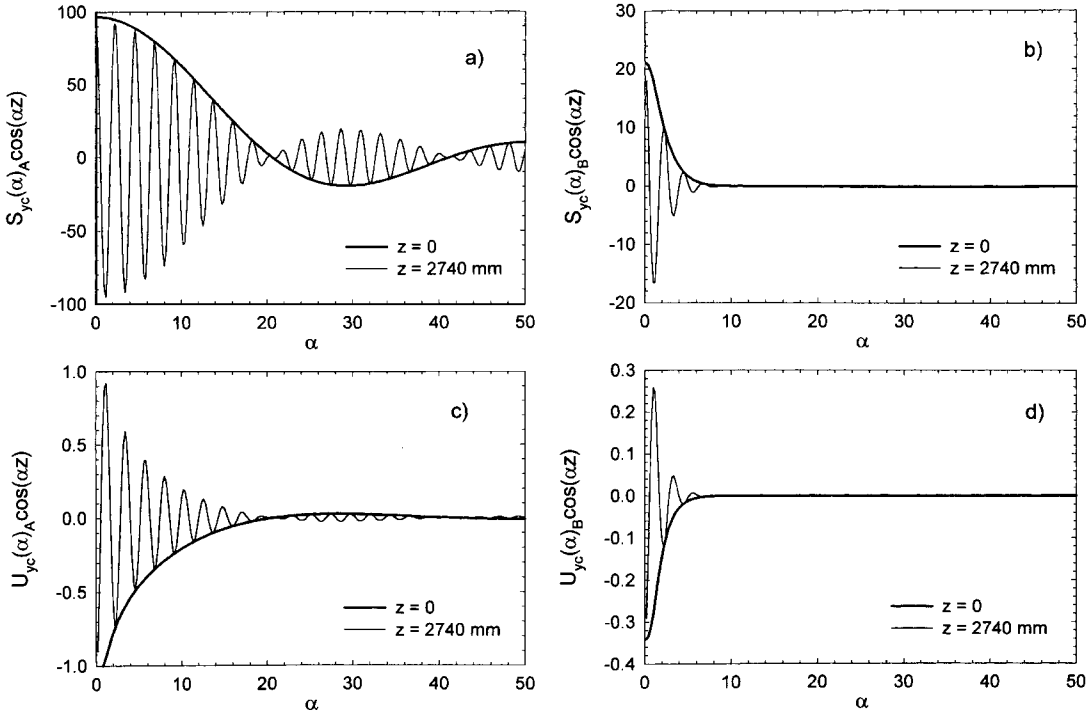

Figure 3. Inverse Fourier integrals for: (a) vertical stress at point A; (b) vertical stress at point B; (c) vertical displacement at point A; and (d) vertical displacement at point B (all with $w = 152$ mm, $z_s = 0$)

Figure 3(b) shows the function to be inverted to obtain the vertical stress at point B (0·9 m below the surface). Significant attenuation with depth occurs in comparison with point A. The magnitude of the stress integrand at point B is roughly one-fifth of that for point A, when α equals zero. More importantly, the magnitude of the stress integrand at point B is essentially zero for α larger than 10. This is in sharp contrast to the periodic function for point A that extends to large values of α.

5.2. *Transformed displacements*

The inverse Fourier integral for vertical displacement $U_{yc}(\alpha)\cos(\alpha z)$ at point A is plotted in Figure 3(c). This integrand is much simpler than that required to invert the transformed loads. The magnitude of the displacement integrand decreases more rapidly for an increase in α than does the load integral. The displacement integrand shown in Figure 3(c) is nearly zero for α larger than 40.

The integrand for the transformed displacements also displays significant attenuation with depth when evaluated at location B (Figure 3(d)). The integrand of the transformed displacements also becomes less complex with depth.

5.3. *Implications for Fourier integral analysis*

Two major conclusions may be drawn from the comparison of the integrands for evaluation of stresses and displacements. First, the Fourier integral of the original load function is more complex than other quantities like displacement since the surface load features a discontinuity. Therefore, the numerical inversion of the transform of surface load is more difficult than other transform quantities. Second, the inversion of stress or displacement quantities at the surface is more difficult than the inversion of those quantities below the surface.

Therefore, the most difficult integrand to integrate numerically would correspond to the inversion of the transform of the original applied load at the surface. This is advantageous as the load variation is known *a priori*. Provided that the numerical inversion is sufficient for this most difficult case, confidence of an accurate solution can be assured for other quantities, both at the surface and at other locations in the ground.

6. NUMERICAL INTEGRATION

Now that the nature of the Fourier integrals has been examined, a discussion of the numerical technique used to perform the inverse integrals is presented. The integration of some function of α between zero and infinity can be performed numerically by first truncating the upper limit of the integrand from infinity to some finite value, and second by evaluating the truncated integral piece wise as a number of sub-integrals, ie.:

$$\int_0^{\infty} f(\alpha)\,\mathrm{d}\alpha \approx \sum_{i=1}^{N} \int_{\Delta\alpha(i-1)}^{\Delta\alpha i} f(\alpha)\,\mathrm{d}\alpha \tag{10}$$

where N is the number of sub-integrals, and $\Delta\alpha$ the width of sub-integral.

Each sub-integral was evaluated using ten point Gaussian integration. Trials were also conducted with two point Gaussian integration which was found to be somewhat less efficient.

The accuracy of the integration is controlled by the number (N) and size ($\Delta\alpha$) of the subintegrals. The selection of these parameters, which determine the upper limit of the integration ($\Delta\alpha \times N$) and the refinement of each sub-integral, is dictated by the need for a solution to be both accurate and efficient.

6.1. Solution of test case–uniformly loaded patch

The trial case involving a uniformly loaded patch ($2w \times 2w$) was also analyzed to investigate the effectiveness of the integration scheme and to verify that correct vertical displacements at the surface were obtained even for large z values away from the load, as required by the particular problem considered by Brachman *et al.*[5]

Since the test problem is symmetric along the lines $x = 0$ and $z = 0$, the vertical deflections along these lines should be the same. This premise was used to test the inversion scheme by comparing the vertical deflections along the line $z = 0$ to those obtained along $x = 0$.

Figure 4(a) plots the sets of vertical deflection results for w of 152 mm. The solid curve represents the deflections obtained in the x–y plane (i.e. along $z = 0$). The other sets are the calculated deflections in the y–z plane (i.e. along $x = 0$) for two different Gaussian quadrature schemes. The prediction with $N = 5$, $\Delta\alpha = 15$ provides reasonable results up to z of 1·8 m, and then differs from the solid curve. The deflections here are essentially zero, however this difference illustrates the effect of large z values on the success of the integration scheme. As previously shown in Figure 3(c), the function to be integrated $U_{yc}(\alpha)\cos(\alpha z)$ becomes more complicated as z increases, consequently a finer sub-integral width is required. Figure 4(a) shows that with $N = 5$ and $\Delta\alpha = 10$, which involves integration with a smaller upper limit, but with greater refinement compared to $N = 5$, $\Delta\alpha = 15$, the correct displacements are obtained for z values up to 3 m.

Figure 4(b) presents the calculated vertical deflections for w of 76 mm. The solid curve again shows the vertical deflection along the line $z = 0$, against which the values obtained along the z-axis will be compared. Curve (ii) presents the deflections obtained using the adopted integration scheme for w of 152 mm (i.e. $N = 5, \Delta\alpha = 10$). These results provide a reasonable estimate of the vertical deflections, however the value at the centre of the patch is slightly overestimated and there is some slight oscillation of the predictions for the higher z values. Curve (iii) shows the consequences of integrating to larger values of α with a coarse sub-integral size. Poor results are obtained with $N = 5$, $\Delta\alpha = 20$, especially for z larger than 1·7 m. Extending the integration scheme to the same α value used for curve (iii) but with twice the number of sub-integrals (i.e. $N = 10, \Delta\alpha = 10$) yields good results up to z of 3 m, shown by curve (iv).

These trial cases confirm that the numerical integration techniques may be successfully used to invert Fourier integrals provided that enough Gaussian quadrature intervals, of small enough size are employed.

7. ANALYSIS WITH MULTI-STEP LOADING

Analysis of multi-step loading (e.g. the two load patches of width w separated by distance $2z_s$, of Figure 1(a)) is more arduous than that for a single patch of pressure. The Fourier cosine integral for the generalized load distribution of Figure 1(a) was given previously in equation (8). The

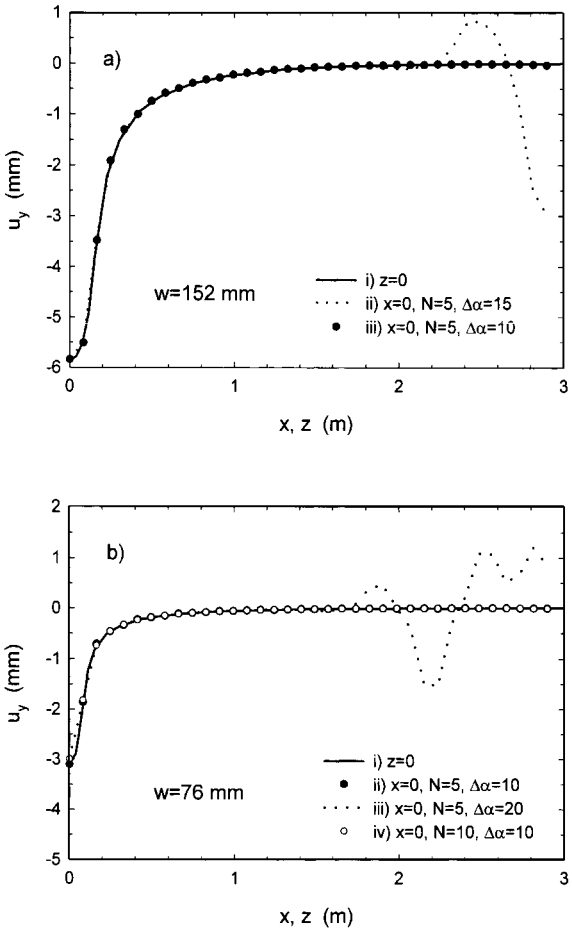

Figure 4. Vertical deflections (u_y) calculated at the surface using different integration schemes for: (a) $w = 152$ mm, and (b) $w = 76$ mm

corresponding equation to invert the transform is

$$f(z) = \frac{2}{\pi} \int_0^\infty \frac{[\sin(z_s\alpha + w\alpha) - \sin(z_s\alpha)]\cos(z\alpha)}{\alpha} \, d\alpha \tag{11}$$

The integrand of equation (11), $g(\alpha)$, is plotted in Figure 5 for cases of $w = 152$, and 76 mm (with $z = 0$). Values are shown for both z_s equal to zero and a large value of z_s. The increased complexity of the integrand for non-zero values of z_s is illustrated in Figure 9. A greater number of zeros result from the $\sin(z_s\alpha)$ components of equation (11) and the amplitude of $g(\alpha)$ is harmonic for non-zero z_s. For locations other than at $z = 0$, $g(\alpha)$ may be even more complex. The additional complexity introduced into the integrand by non-zero z_s values means that greater computational effort is needed to invert the transform.

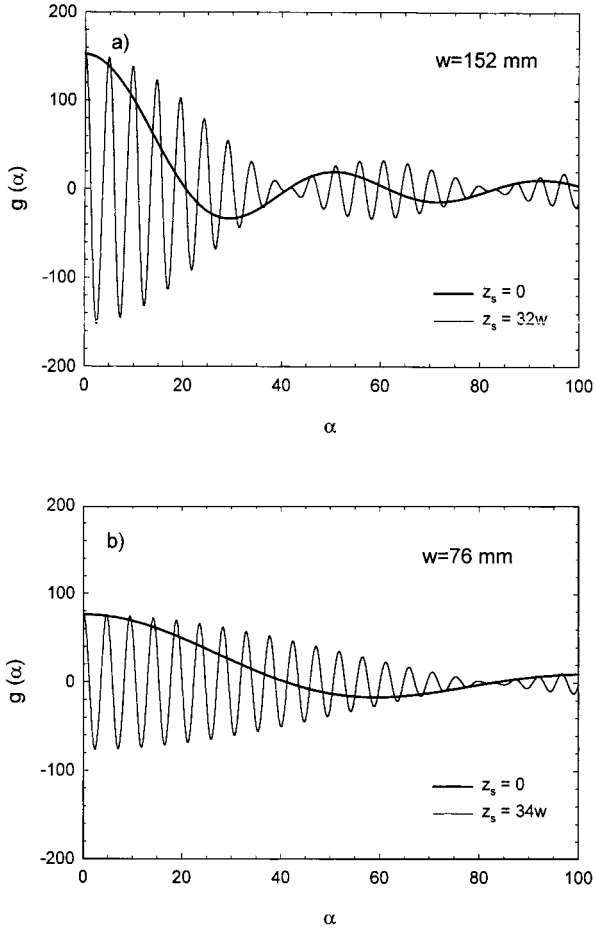

Figure 5. Inverse Fourier integrals for multi-step load variation showing effect of non-zero z_s (calculated at $z = 0$) for: (a) $w = 152$ mm, and (b) $w = 76$ mm

The transform of the load function becomes increasingly complex for the case of large z_s relative to w. When evaluating inverse integrals for large z_s relative to w, it was found to be considerable more efficient to employ superposition to assemble the solution for the multi-step load variation from two simpler solutions with z_s equal to zero. For example, solution efficiency was improved by considering the response to a load with half-width $(z_s + w)$ minus the response to a load with half-width (z_s), rather than by direct evaluation of the load case shown in Figure 1(a).

SUMMARY AND CONCLUSION

The nature of the inverse integrals and the numerical integration required to employ Fourier integral analysis of three-dimensional problems has been described. These integrals may be

complex functions for the generalized load function considered, particularly for evaluation at non-zero longitudinal positions ($z \neq 0$) and for patches separated by distance z_s.

The Fourier integral of applied load is more complex and thus more difficult to invert than those for stresses and displacements. Since the applied load is known *a priori*, integration schemes can be selected that provide accurate and efficient inversion of the original load function. This assures correct stresses and displacements throughout the elastic body. The complexity of Fourier integrals of stress and displacement decreases significantly with depth. Accuracy of Fourier integral inversions therefore improves as depth increases below the applied loading.

The use of piece-wise Gaussian integration over a truncated region provides good results provided that sufficient number and refinement of sub-integrals is selected. For the case of a simple loaded area, these choices depend on the relative magnitude of load width w and maximum longitudinal co-ordinate (maximum z-value). For multi-step loads integration must be refined to account for the additional complexity of the inverse integrals. For cases with loaded areas separated by large distances (relative to the load width) the use of superposition involving load components with less complex inverse integrals is beneficial.

ACKNOWLEDGEMENTS

This work has been supported by the Natural Sciences and Engineering Research Council of Canada through a PGS-B scholarship awarded to Mr. Brachman and a research grant awarded to Dr. Moore.

REFERENCES

1. J. C. Small and W. K. Wong, 'The use of integral transforms in solving three dimensional problems in geomechanics', *Comput. and Geotech.* **6**(3)**,** 199–216 (1988).
2. I. D. Moore and R. W. I. Brachman, Three-dimensional analysis of flexible circular culverts', *J. Geotech. Engng.*, **120**(10)**,** 1829–1844 (1994).
3. R. W. I. Brachman, I. D. Moore and R. K. Rowe, Interpretation of a buried pipe test: small diameter pipe in the Ohio University facility', Transportation Research Record, Vol. 1541, 1996, pp. 64–70.
4. N. S. M. Fernando, J. C. Small and J. P. Carter, 'Elastic analysis of buried structures subject to three-dimensional surface loading', *Int. J. Numer. Anal. Meth. Geomech.*, **20,** 331–349 (1996).
5. R. W. I. Brachman, I. D. Moore and R. K. Rowe, Analysis of pipe structures in soil test cells — Ohio University Facility, Geotechnical Research Centre *Report GEOT-14-95*, The University of Western Ontario, 96 p.

